Biomaterials Science

ROYAL SOCIETY OF CHEMISTRY

PAPER

View Article Online
View Journal

Cite this: DOI: 10.1039/d5bm01612f

Bioinspired synergistic chitosan–graphene–tannin hydrogel orchestrates inflammation resolution and accelerates skin tissue repair

Isleidy Ruíz, *[a] Luisbel González, [b] Julia Eduarda Schneider Gregória,[c,d] Cintia Sena Bueno,[c,d] Maria Esméria Corezola do Amaral,[c,f] Guilherme Ferreira Caetano*[c,d,e] and Katherina Fernández*[a]

Wound healing remains a major clinical challenge due to the complex metabolic disturbances present within the wound microenvironment. In this study, we report the development and comprehensive validation of a novel multifunctional hydrogel composed of chitosan (CS), reduced graphene oxide (rGO), and tannins (TA) (CS-rGO-TA), specifically engineered as an advanced wound dressing. The hydrogel was thoroughly characterized using SEM to examine its porous microstructure, FTIR to analyze component interactions, the DPPH assay to assess antioxidant capacity, and total phenols to evaluate the release kinetics of TA. Antibacterial activity was tested *in vitro* against *Escherichia coli* and *Staphylococcus aureus* using standard colony-forming unit assays. Biocompatibility and regenerative potential were assessed through cell viability and migration assays using human dermal fibroblasts. *In vivo* evaluation included a skin irritability model in guinea pigs and a full-thickness excisional wound model in rats, divided into four treatment groups. Wound closure progression was monitored over time, and histological analysis was performed using hematoxylin and eosin (H&E), Mallory, and Masson's Trichrome staining to assess tissue morphology and collagen deposition. The CS-rGO-TA_3 hydrogel demonstrated controlled and sustained TA release, strong antioxidant and antibacterial properties, and excellent biocompatibility, with no signs of irritation or adverse effects. Its application significantly accelerated wound closure and promoted organized deposition of collagen (types I and III). Molecular analysis revealed early resolution of inflammation, enhanced angiogenesis, and polarization of macrophages toward a reparative M2 phenotype, as evidenced by modulation of markers such as MPO, CD68, ARG1, and interleukins IL-6, IL-10, IL-1β, and IL-1rn. Collectively, these findings highlight the CS-rGO-TA_3 hydrogel as a safe and effective therapeutic platform with strong potential for tissue regeneration and clinical wound management.

Received 4th November 2025,
Accepted 9th April 2026

DOI: 10.1039/d5bm01612f

rsc.li/biomaterials-science

1. Introduction

Wound healing treatment has evolved significantly over the years, prompting the search for innovative and effective treatment modalities.[1] Among the numerous advancements in this field, wound dressings have gained considerable attention for their ability to facilitate the healing process and minimize complications. Hydrogel dressings have emerged as a promising solution for wound healing due to their ability to provide a moist environment that facilitates the healing process.[2,3] This property helps absorb wound exudate and allows for shape adaptation, which is beneficial for wounds in areas of constant movement, offering significant advantages over traditional dry dressings, which often lack functionality and can cause pain upon adhering to the wound.[4–6] Hydrogels can also be modified to incorporate active compounds such as growth factors and antibacterial compounds, which enhances their effectiveness in wound healing.[7,8] Furthermore, they can be designed to be self-adhesive, antioxidant, and self-healing, which prolongs their lifespan and improves wound protection.[9,10]

Chitosan (CS) is an alkaline polysaccharide obtained from the partial deacetylation of chitin present in some crustaceans.[11] CS is a biopolymer distinguished by its anti-

[a]*Laboratorio de Biomateriales, Departamento de Ingeniería Química, Facultad de Ingeniería, Universidad de Concepción, Concepción, Chile. E-mail: isruiz@udec.cl, kfernandeze@udec.cl*
[b]*Instituto de Ciencias Aplicadas, Facultad de Ingeniería, Universidad Autónoma de Chile, Santiago 8581151, Chile*
[c]*University Center of Hermínio Ometto Foundation, FHO, Araras 13607-339, Brazil. E-mail: caetanogf@fho.edu.br*
[d]*Graduate Program of Orthodontics, University Center of Hermínio Ometto Foundation, FHO, Araras 13607-339, Brazil*
[e]*Division of Dermatology, Department of Internal Medicine, Ribeirao Preto Medical School, University of Sao Paulo, Sao Paulo 05508-060, Brazil*
[f]*Núcleo de Ciência da Saúde-Centro Universitário da Fundação Hermínio Ometto, Araras, SP, Brasil*

microbial,[12] biodegradable,[13] and non-toxic[14] properties, in addition to possessing excellent biocompatibility,[15] mucoadhesive properties,[16] limited immunological reactions,[17] and characteristics that favor absorption.[18] Thanks to its remarkable biological properties, such as promoting blood coagulation, promoting fibroblast proliferation, and collagen formation, CS contributes to improving the wound healing process.[19] Despite their benefits, CS hydrogels often face challenges related to their mechanical properties, so the incorporation of nanomaterials and biomolecules is a promising strategy to improve or generate new functions in these hydrogels. Reduced graphene oxide (rGO) offers a multifaceted approach for the synthesis of new hydrogels.[20] Hydrogels containing rGO possess good mechanical,[21] conductive properties[22] and antibacterial activity,[23] combined with their ability to promote angiogenesis, cell proliferation, and migration in the wound healing process.[24] The hydrogel composed of CS/RGO and an electrolyzed polycaprolactone and cellulose acetate membrane designed by Graça *et al.* (2022) demonstrated the ability to provide a moist environment, prevent exudate accumulation, and allow gas exchange, as well as act as a barrier against bacterial penetration and show cell viability greater than 90% against human dermal fibroblast cells.[25] modern hydrogels are designed with antibacterial and antioxidant properties, which are crucial for preventing infection and promoting faster healing.[26] Recent research highlights the potential of incorporating natural biopolymers, such as tannins (TA), into these dressings to enhance their therapeutic properties.[27]

The TA, a polyphenolic family, exhibits a variety of properties that significantly contribute to their use in wound dressings. Primarily known for their astringent qualities, TAs facilitate tissue regeneration by precipitating proteins, which improves the healing process and reduces inflammation.[28] Furthermore, their antioxidant properties play a crucial role in mitigating oxidative stress, a detrimental factor in wound healing.[29] The incorporation of TAs into wound dressings has been shown to improve the overall efficacy of the dressing, offering not only protection against pathogens but also promoting moisture retention, which is essential in moist wound healing environments.[30] Carrasco *et al.* (2024) incorporated rGO and TA into an alginate-based hydrogel, achieving significant improvements in mechanical strength, tissue adhesion, and cell viability, with no observed cytotoxic effects.[31]

Building upon these findings, this study presents the development and validation of a novel multifunctional hydrogel composed of tannin-loaded chitosan-reduced graphene oxide (CS-rGO-TA), specifically designed to address the multifaceted biological challenges associated with impaired wound healing. By integrating the biocompatibility and fluid absorption capacity of CS, the mechanical reinforcement and angiogenic potential of rGO, and the potent antibacterial, antioxidant, and anti-inflammatory properties of TA, this hydrogel provides a synergistic platform that addresses key pathological barriers in both chronic and acute wounds. A major novelty of this work lies in the rational design that enables not only structural support and protection but also active immunomodulation, particularly through the sustained release of TAs, which promotes a macrophage phenotypic switch from pro-inflammatory M1 to reparative M2 states. This is supported by both molecular and histological evidence, a mechanistic insight rarely emphasized in prior hydrogel research. Additionally, the combination of these three components results in enhanced antibacterial efficacy, collagen organization, and vascularization; achievements not observed in hydrogels containing only one or two of these materials. The comprehensive *in vitro* and *in vivo* validation, including western blot, RT-PCR, and immunohistochemistry, further substantiates the therapeutic superiority of CS-rGO-TA over conventional formulations. Altogether, this hydrogel represents a significant advancement in the development of bioengineered wound dressing, offering a multifunctional, immunoresponsive, and tissue-regenerative alternative with broad potential for clinical translation.

2. Materials and methods

2.1. Materials

Graphite powder (flakes, 325 mesh) was purchased from Asbury Online (Asbury Carbons, NJ, USA). Low molecular weight chitosan (CS) with a Brookfield viscosity of 200–800 cP (CAS number 9012-76-4) and Pluronic F 127 (PF) (PEO_{97}-PPO_{69}-PEO_{97}) (CAS number 9003-11-06) were purchased from Sigma Aldrich Chemicals (Chile, South America). Phosphoric acid (H_3PO_4), sulfuric acid (H_2SO_4), potassium permanganate powder ($KMnO_4$), hydrogen peroxide (H_2O_2, 30%), hydrochloric acid (HCl), ethanol (C_2H_5OH), tris ($(HOCH_2)_3CNH_2$), dopamine hydrochloride (DA-HCl, minimum 98%), sodium hydroxide (NaOH), silver nitrate ($AgNO_3$), Dulbecco's modified Eagle's medium (DMEM), dimethyl sulfoxide (DMSO), 3-(4,5-dimethylthiazol-2-yl)-2,5-diphenyltetrazolium bromide reagent (MTT), phosphate-buffered saline (PBS), and fetal bovine serum (FBS) were purchased from Sigma-Aldrich Company (St Louis, MO, USA). All reagents and solvents were of analytical grade and used without further purification. Milli-Q® water was used throughout the study.

2.2. Synthesis of hydrogels CS-rGO-TA

First, CS (1.5 g) was dissolved in 50 mL of 1% HCl to obtain a 3% w/v solution. In parallel, rGO (0.25 g) was dispersed in 50 mL of Milli-Q® water by sonication for 2 h, yielding a 0.5% w/v dispersion. A Pluronic F-127 (PF) solution (1% w/v; 0.5 g in 50 mL of PBS) was also prepared. The CS and rGO solutions were mixed in a 1 : 1 (v/v) ratio under stirring (1 h, 650 rpm) and subsequently cooled to 4 °C to facilitate physical crosslinking. PF was then incorporated at 10% (v/v) relative to the CS–rGO mixture and stirred for an additional 20 min. TA was added at concentrations of 1%, 3%, and 5% (w/v) with respect to the final formulation and stirred vigorously for 1 h. The mixture was subsequently sonicated for 30 min to remove entrapped air bubbles and incubated at 37 °C until complete gelation. Based on this preparation, the final hydrogel composition corresponded to approximately 0.3 g of CS and 0.05 g of

rGO per formulation, with TA contents of 0.0035 g (1%), 0.0105 g (3%), and 0.0175 g (5%). These values correspond to final concentrations of approximately 0.6% (w/v) of CS and 0.1% (w/v) of rGO in the hydrogel matrix, ensuring the reproducibility of the formulation. The relative proportions of each component remained constant in all formulations, with the TA concentration being the only variable parameter. The resulting hydrogels were designated CS-rGO-TA_1, CS-rGO-TA_3, and CS-rGO-TA_5, respectively. The rGO and TA used in this study were synthesized at the Biomaterials Laboratory of the University of Concepción, and detailed synthesis and purification protocols are provided in the SI.

2.3. Characterization of hydrogels CS-rGO-TA

2.3.1. Scanning electron microscope (SEM). The micromorphology of hydrogel composites was evaluated by SEM analysis. SEM images were recorded using a JEOL JSM-6380LV, Japan model microscope at 10 kV. The hydrogels were coated using a gold sputter coater and their surfaces were observed at different resolutions (4 μm, 20 μm and 50 μm).

2.3.2. FT-IR spectroscopy. The FT-IR was used to investigate the chemical interaction between the material's composites. The PerkinElmer UATR Two FTIR Spectrometer (USA) recorded the spectra. The wavenumber range analyzed was 4000–500 cm^{-1}, and 40 accumulated scans were acquired.

2.3.3. Drug release capacity. Samples of the previously synthesized hydrogels (0.5 cm^2) were taken and weighed to determine their mass (mH). They were then placed in 50 mL of PBS and stirred at 37 °C, pH 7.4, at a speed of 60 rpm. At specific time intervals, 100 μL of the soaking solution was collected, and the TA absorbance at 765 nm was measured by UV-Vis spectrophotometry (Techcomp, UV2300, China). The TA concentration was determined from the standard curve, and the mass of TA released from the hydrogel (mH) was indirectly calculated. The release rate of the CS-RGO-TA hydrogels was calculated according to eqn (1). The samples were analyzed in triplicate.

$$\text{Release rate } (\%) = m_H/m_a \times 100 \quad (1)$$

2.3.4. Antioxidant capacity. Antioxidant activity was measured by an *in vitro* DPPH. The antioxidant capacity of the hydrogels was evaluated by their ability to scavenge DPPH free radicals. First, a 0.1 mM DPPH solution in ethanol was prepared as a working solution. Next, 20 mg of hydrogel was dissolved in 2 ml of this DPPH working solution and incubated for 1 h in the dark. After incubation, the supernatant was collected, and the absorbance at 517 nm was measured using a UV-Vis spectrophotometer (Techcomp, UV2300, China). The DPPH free radical scavenging activity was calculated by eqn (2):

$$\text{Scavenging activity } (\%) = A_{blank} - A_{sample}/A_{blank} \times 100 \quad (2)$$

where A_{blank} and A_{sample} are the absorbance values of the DPPH working solution and the sample, respectively. Each sample was analyzed in triplicate. All experiments were conducted at room temperature, atmospheric pressure, and 85% humidity.

Biocompatibility of hydrogel. The cytotoxicity of the hydrogels was determined using the 3-(4,5-dimethylthiazol-2-yl)-2,5-diphenyltetrazolium bromide (MTT) assay and cell migration was assessed using a scratch assay. Human dermal fibroblasts were used to assess the *in vitro* cytotoxicity and cell migration of all synthesized materials. Details of the *in vitro* characterizations are described in the SI.

2.3.5. Antibacterial activity *in vitro*. The antibacterial activity of the hydrogels was evaluated *in vitro* using *Escherichia coli* (*E. coli*, ATCC 27195) and *Staphylococcus aureus* (*S. aureus*, ATCC 25923) strain models, 200 μL of the hydrogels were inoculated with a bacterial suspension of 10 μL at a concentration of 10^6 CFU mL^{-1} in 48-well plates and incubated at 37 °C for 3 hours. Sterile PBS (1 mL) was added to the plate to resuspend the surviving bacteria. Agar plates were coated with 20 μL of the bacterial resuspension to evaluate antibacterial activity. These plates were then incubated at 37 °C for 16 hours. A bacterial suspension of 10 μL at 10^6 CFU mL^{-1} in sterilized PBS (1 mL) served as the control group. After incubation, colony-forming units were counted visually. The antibacterial activity of the hydrogels was expressed as a percentage of bacterial death (eqn (3)).

$$\text{Kill } (\%) = (N_{control} - N_{hydrogel})/N_{control} \times 100 \quad (3)$$

where $N_{control}$ was the colony-forming units of control and $N_{hydrogel}$ was the survivor count on hydrogels. The experiments were carried out in triplicate.

2.4. Animal experiments

All animal procedures were performed in strict accordance with the Experimental Standards and Biodiversity Rights (NIH publication 80–23, revised in 1996, and Arouca Law 11,794, 2008) for the Care and Use of Laboratory Animals. The experimental protocol was reviewed and formally approved by the Animal Ethics Committee of the University Centre of the Herminio Ometto Foundation (protocol approval number: 003/2024). All efforts were made to minimize animal suffering and to reduce the number of animals used in accordance with the 3Rs (Replacement, Reduction, and Refinement) principles.

2.4.1. Irritability assessment. The irritation potential of the hydrogels was evaluated in five Guinea pigs (Cavia porcellus, 300–500 g body weight). The procedure began with the administration of anesthesia using ketamine (40–50 mg per kilogram) and xylazine (4–5 mg per kilogram). The dorsal surface of each animal was shaved for 24 h, and two pieces of the material were placed on the shaved skin. The hydrogels were then covered with a transparent dressing (3M Tegaderm™, USA) for a total of 12, 24, 48, and 120 h, after which the dressing was removed and dermal reactions, including erythema, eschar, and edema, were scored according to established guidelines (Table S1). A group of three untreated animals served as controls. After 5 days, the animals were euthanized by CO_2 inhalation in a euthanasia chamber, followed by cervical dislocation.

2.4.2. Evaluation of the healing potential of hydrogel in the rat dorsal skin wound model. Wound healing was studied

in 36 male Wister rats (mean weight 190–210 g), divided into 4 groups and 3 experimental times (2, 7, and 14 days). The wound healing rate (WHR) of the different groups was assessed by clinical and photographic evaluation of the wounds, and the evolution of the injured areas was recorded using ImageJ software. Finally, all wound biopsies were collected for subsequent histological analysis. Details of the *in vivo* characterizations are described in the SI.

2.4.3. Histological analysis. The excised wound tissues were fixed in 10% (v/v) formalin solution, dehydrated through a graded alcohol series (50–100% (v/v)), cleared in xylene, and embedded in paraffin. Serial 4.0 μm-thick sections were cut using a microtome and stained with hematoxylin and eosin (H&E) (assessment of inflammatory infiltrate). The slides were then stained with Mallory and Masson's Trichrome staining (collagen formation evaluation) and examined under a light microscope using Leica Application Suite version 3.2.0 software. For each wound skin sample from each animal, six sections were taken and examined (400× magnification). Collagen formation was quantified using the "Color Deconvolution" plugin in ImageJ software, where the three colors of the trichrome stain were deconvolved. Only the percentage of the total blue area (collagen) in the image was determined. The results were expressed as the average collagen distribution per treatment.

2.4.4. Molecular analysis by western blot. The quantified proteins (50 μg of total proteins) were electrophoresed on a 12% polyacrylamide gel (SDS-PAGE) using the BioRad minigel apparatus with electrophoresis buffer. Transfer of the separated proteins in the gel was performed electrically to a nitrocellulose membrane using a Bio-Rad® device for approximately 1.5 hours at 120 V, with the membrane kept on ice. The primary antibodies used are described in Table S2. Optical density was read using ImageJ® software. The results were normalized by comparing the expression with GAPDH. Details of the test procedure are described in the SI.

2.4.5. RNA extraction and RT-qPCR. Total RNA from samples collected at 30 days postoperatively was macerated in liquid nitrogen and isolated using TRIzol™ reagent (Invitrogen, Waltham, MA, USA) for RNA isolation, following the manufacturer's instructions. According to the manufacturer's instructions, RNA was converted to cDNA from 1.5 μg of total RNA using the High-Capacity Kit (Thermo Fisher Scientific, Waltham, MA, USA). The TaqMan assays used are described in Table S2 and were purchased from Applied Biosystems. Reactions were performed in triplicate with TaqMan Gene Expression Master Mix (Applied Biosystems, Waltham, MA, USA). The entire qPCR procedure was performed according to the previously described protocol.[32] GAPDH was used as a control for data normalization and validated using BestKeeper software. The PCL group was used as a calibrator, and the results were calculated using the $2^{-\Delta\Delta Ct}$ method.

2.5. Statistical analysis

Students' *t*-test was used to compare each experimental group with the control group. Different letters indicate statistically significant differences between groups ($p < 0.05$, one-way ANOVA with Tukey's *post hoc* test). Graphs and statistical analyses were performed using Statgraphics Centurion® XVII software.

3. Results and discussion

To understand the structural design and functional integration of the CS-rGO-TA hydrogel, a schematic representation of the polymer network is presented, describing the main physicochemical interactions responsible for its formation and stability. This illustration allows visualization of the molecular interactions between CS, rGO, and TA, which support the generation of a stable, interconnected, and multifunctional hydrogel matrix (Fig. 1). Based on this conceptual framework, a mor-

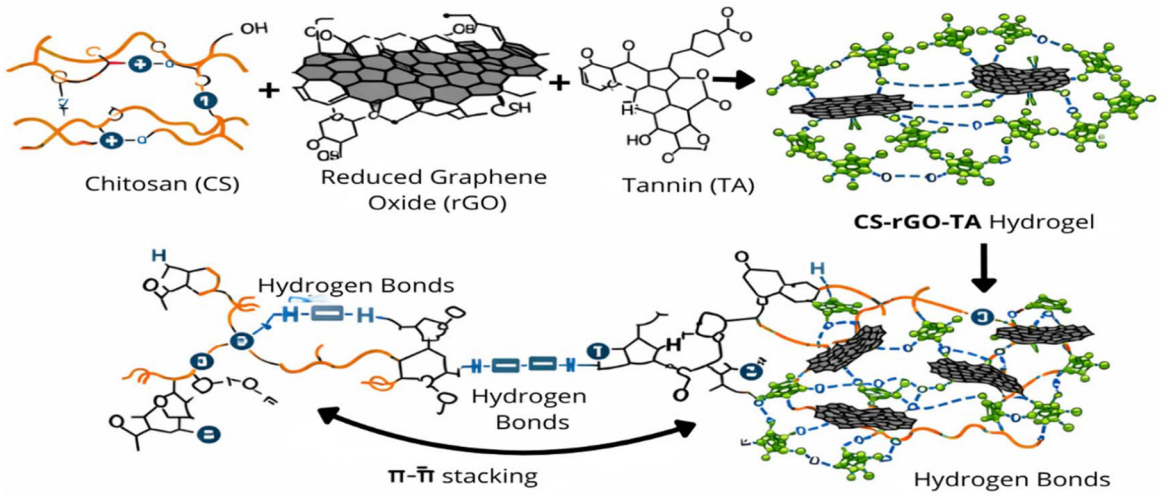

Fig. 1 Schematic representation of the CS-rGO-TA hydrogel network. Source: own elaboration.

phological and physicochemical characterization was subsequently carried out, aimed at correlating the proposed network architecture with its structural, mechanical, and biological properties. Together, these analyses provide a comprehensive understanding of how the hydrogel's composition and organization contribute to its performance as an advanced wound-healing platform.

During hydrogel formation, rGO acts as a nanoreinforcement within the CS network, forming π–π interactions and hydrogen bonds with the CS chains. These interactions restrict the mobility of the polymer matrix, leading to an increase in the elastic modulus and overall mechanical strength.[33] Furthermore, the TA acts as a polyphenolic crosslinker, capable of forming supramolecular networks through multiple hydrogen bonds, and, in some systems, this increases the crosslinking density and reinforces the mechanical integrity of the gel. The use of TA as a crosslinking agent in CS matrices or other hydrophilic polymers has been widely documented.[34–36] CS forms a cationic polymer matrix that interacts with rGO nanosheets *via* hydrogen bonds and electrostatic interactions,[37] while TA acts as a multifunctional polyphenolic crosslinker *via* hydrogen bonds and π–π interactions.[38] The hydrogel network is stabilized primarily through non-covalent interactions, including hydrogen bonds, π–π stacking between rGO and the aromatic rings of TA, and electrostatic interactions between the protonated CS chains and the rGO nanosheets. The synergistic assembly generates a dense supramolecular network that improves mechanical strength, modulates swelling, and promotes sustained release, as presented in Fig. 1.

3.1. Physicochemical characterization

The surface morphology of the hydrogels was observed by SEM (Fig. S1). All hydrogels exhibited rough surfaces characterized by well-defined lamellae and amorphous structures, attributable to the varied interactions between the constituent raw materials. Notably, increasing TA content led to denser surface morphology, which is likely due to a higher crosslinking density resulting from enhanced hydrogen bonding and hydrophobic interactions involving the PF.

FTIR analysis was performed to investigate the chemical composition and successful integration of the hydrogel components. The FTIR spectrum of pure CS displayed its characteristic absorption bands, including broad peaks corresponding to hydroxyl (–OH) groups, primary amines, the C=O stretching of amide I, and the C–O–C stretching and N–H bending vibrations of amide II (Fig. S2A).[39–41] The effective reduction of graphene oxide (GO) and subsequent functionalization of rGO with dopamine (DA) amino groups were confirmed by the appearance of distinct absorption bands at 1220 cm^{-1} and 1050 cm^{-1}, respectively.[42–44] The spectrum of TA revealed prominent bands attributed to both aromatic and non-aromatic hydroxyl groups, C=O stretching vibrations, and C–O stretching modes in aromatic and aliphatic structures.[45] The PF spectrum exhibited characteristic peaks corresponding to CH_2 and CH stretching vibrations, along with distinct signals attributed to C–O–C and C–O bond stretching.[46,47] In the synthesized hydrogels (Fig. S2A), the characteristic bands of CS and rGO were retained, and the intensity of TA-related peaks increased progressively with higher TA concentrations. These spectral features confirm the successful incorporation of TA into the hydrogel matrix and the preservation of essential functional groups from each component, supporting the structural integrity and multifunctional nature of the final formulation.

In previous studies,[48] the synthesis of the hydrogel was optimized using a Central Composite Design (CCD) statistical design and Response Surface Methodology. Its physicochemical characterization was also carried out, obtaining representative values for electrical conductivity using the four-point method (2.30 mS cm^{-1}), swelling capacity in simulated fluids (577.42%), and mechanical properties determined by tensile testing, including tensile strength (22.14 MPa) and elastic modulus (169.97 MPa). The obtained conductivity is consistent with that of other CS/rGO-based hybrid hydrogels, which are typically in the range of 1.8–3.5 mS cm^{-1}, depending on the degree of GO reduction and the quality of its dispersion. Table 1 presents a comparison of the physical properties of the CS-rGO-TA hydrogel with representative CS/graphene oxide hydrogel systems described in the literature.

Chitosan-based materials crosslinked with condensed polyphenols exhibit swelling capacity values comparable to those obtained in this study, suggesting that the supramolecular interaction between phenolic hydroxyl groups and polymer chains favors a structural network with a suitable balance between mechanical stability and fluid absorption.[54,55] As

Table 1 Comparison of the physical properties of the CS-rGO-TA hydrogel with representative CS/graphene-based hydrogels reported in the literature

Hydrogel system	Electrical conductivity (mS cm^{-1})	Swelling ratio (%)	Tensile strength (MPa)	Elastic module (MPa)	Reference
CS-rGO-TA_3 (this work)	2.30	577	22.14	169.97	This study
CS-GO-DA	0.8–1.2	420–580			Jing *et al.*, 2017[49]
CS-rGO-PDA		200–320		0.2–0.5	Li *et al.*, 2024[50]
CS-rGO hydrogel			0.07–0.09	0.12–0.17	Graça *et al.*, 2023[51]
CS-GO		200–400	20.96	0.364	Nath *et al.*, 2018[52]
CS-GO-gelatin		800–900	10–14 MPa	0.1–0.3	Li *et al.*, 2023[53]

described in systems reinforced with graphene nanomaterials, the incorporation of rGO reduces swelling due to increased polymer network stiffness and decreased chain mobility.[56] Indeed, the swelling observed in our system is consistent with that of hydrogels with moderate-to-high crosslinking density, supporting the proposed structural interpretation for CS-rGO-TA. Regarding mechanical properties, the tensile strength and elastic modulus values coincide with those reported for rGO-reinforced hydrogels and polyphenol-crosslinked hydrogels, which exhibit a significant increase in stiffness and mechanical support capacity due to the dual reinforcing effect of rGO and TA.[37,57–59] Consequently, the results confirm that both components effectively contribute to the mechanical reinforcement of the hydrogel without compromising the flexibility required for its application in wound healing. These properties demonstrate the formation of a polymer network with mechanical and transport characteristics suitable for biomedical applications, particularly in tissue engineering and skin repair. These properties are fundamental to ensuring the material's structural stability and guaranteeing its ability to maintain a moist and bioactive microenvironment in direct contact with the injured tissue. Based on this, the present study advances the *in vivo* validation of the hydrogel's therapeutic potential, specifically evaluating its effect on the healing process. The analysis focuses on determining how the incorporation of tannins modulates the tissue response, considering that these phenolic compounds possess recognized anti-inflammatory, antioxidant, and antimicrobial properties.

3.2. TA release assays

TA release from the hydrogels was evaluated in PBS (pH 7.4), as shown in Fig. S3. The release profiles demonstrated sustained and prolonged release, indicating controlled release kinetics. Among the formulations tested, the CS-rGO-TA_3 hydrogel showed the highest cumulative release, reaching approximately 23% in the first hour. This controlled release behavior is likely attributed to the stronger interactions between the polyfunctional components and TA, as well as the denser network structure of the composite hydrogel, which regulates diffusion. In terms of antioxidant performance, the CS-rGO hydrogel showed minimal free radical scavenging activity (3%). In contrast, the TA-loaded hydrogels showed a substantial improvement in antioxidant capacity, with CS-rGO-TA_3 achieving the highest activity at 19%. Although the cumulative release of TA reached only 23% after 1 h, this fraction is sufficient to generate therapeutic concentrations in the wound microenvironment. TA exerts potent antioxidant and anti-inflammatory activity at low μg ml^{-1} levels, and the accelerated initial release provides rapid modulation of ROS and pro-inflammatory cytokines.[26,60,61] This behavior is consistent with that reported by González *et al.* (2026), who observed that an early release of 20–30% TA from collagen-rGO hydrogels was sufficient to induce rapid and sustained biological effects.[62] The sustained release of TA from the hydrogel matrix likely helps mitigate cell damage induced by oxidative stress, thereby supporting and accelerating tissue repair.[63]

3.3. Antibacterial activity

The ability to inhibit microbial growth is a crucial characteristic of effective wound dressings. In this study, the bactericidal activity of hydrogels was evaluated against two representative pathogens: *Escherichia coli* (a Gram-negative bacterium) and *Staphylococcus aureus* (a Gram-positive bacterium). Antibacterial efficacy was quantified as $\log_{10}$ reduction values derived from CFU measurements (Fig. 2A and B). The CS-rGO hydrogel exhibited a moderate antibacterial effect, achieving approximately 1.1 $\log_{10}$ reduction against *E. coli* and 1.3 $\log_{10}$ reduction against *S. aureus* compared to the untreated control. Notably, the TA-loaded formulation (CS-rGO-TA_3) showed improved antibacterial performance, reaching approximately 1.7 $\log_{10}$ reduction for *E. coli* and 2.0 $\log_{10}$ reduction for *S. aureus*. These results indicate that the incorporation of tannins enhances bacterial inhibition, particularly against Gram-positive bacteria. Importantly, these values correspond to a moderate antibacterial effect and should not be interpreted as complete bactericidal activity. Although the CS-rGO-TA_3 hydrogel exhibited higher log-reduction values than CS-rGO, the difference was not statistically significant, suggesting that TA provides an additive contribution rather than a fully synergistic effect. The greater susceptibility of *S. aureus* compared to *E. coli* is consistent with previous reports and can be attributed to differences in cell wall structure, where the outer membrane of Gram-negative bacteria acts as an additional barrier to antimicrobial agents. The antibacterial activity of the hydrogels can be explained by the combined action of their components. CS exerts antimicrobial effects through electrostatic interactions between its protonated amino groups and negatively charged bacterial membranes, leading to membrane destabilization and cell death.[64] rGO contributes through physical disruption of bacterial membranes and the induction of oxidative stress *via* reactive oxygen species generation.[65] The incorporation of TA further enhances this effect by interacting with bacterial proteins, disrupting metabolic pathways, and contributing to the local redox balance.[66,67] Overall, the CS-rGO-TA_3 hydrogel exhibits superior antibacterial performance compared to the CS-rGO system; however, its activity falls within a moderate logarithmic reduction range. Consequently, these results should be interpreted as evidence of improved antibacterial functionality, rather than complete eradication of the bacterial load. This behavior is consistent with that reported for chitosan-based hydrogels loaded with polyphenolic compounds. In this context, Li *et al.* (2023) demonstrated that the incorporation of TA into CS matrices increases antibacterial efficacy compared to formulations without this condensed polyphenol, which supports the contribution of TA observed in the present study.[68]

3.4. Cell viability and migration assay

Biocompatibility is a critical factor in the design of wound dressings, as it directly influences cellular responses and tissue regeneration. To evaluate the biocompatibility of the TA-

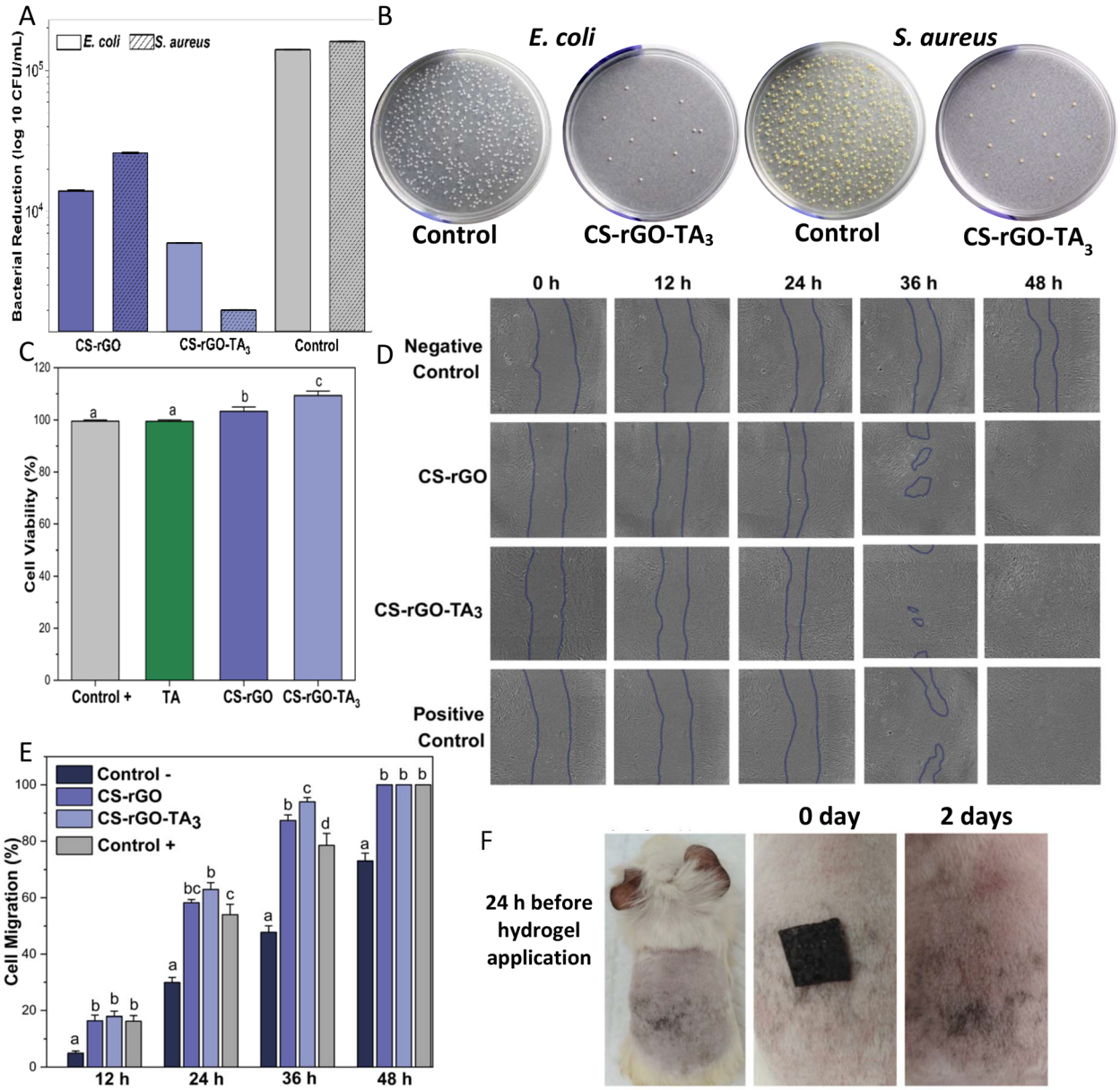

Fig. 2 *In vitro* characterization and irritation potential assay. *In vitro* antibacterial activities of synthesized hydrogels: *S. aureus* and *E. coli* killing ratio (A), photographs of *S. aureus* and *E. coli* colonies on agar plates (B). *In vitro* characterization of human dermal fibroblast cells in the presence of synthesized hydrogels: cell viability (C), wound closure rate over time (D), and images of wound closure at 0, 12, 24, 36, and 48 hours (E). Images of the dermal irritability assay in Guinea pigs (F). Results were expressed as mean ± standard error of the mean (significance levels were set at $p < 0.05$, and differences were considered significant when the groups compared displayed different letters).

enhanced hydrogel (CS-rGO-TA_3), *in vitro* cytotoxicity assays were performed using human dermal fibroblasts (HDFs). The results showed that HDF viability exceeded 100% after 24 hours of incubation (Fig. 2C), indicating not only the absence of cytotoxic effects but also a stimulatory influence on cell proliferation. Interestingly, the incorporation of TA significantly improved cell viability, suggesting that the CS-rGO-TA_3 hydrogel creates a favorable environment for fibroblast activity and wound repair. Fibroblasts play a central role in wound healing by producing collagen fibers and extracellular matrix components, thereby supporting granulation tissue formation and structural tissue remodeling.[69] To assess the hydrogel's effect on fibroblast migration, a scratch assay was conducted (Fig. 2D and E).

During the first 12 hours post-injury, wounds treated with the hydrogels exhibited closure rates comparable to those of the positive control and significantly greater than those observed in the untreated negative control (Fig. 2D). At 24 and 36 hours, cell migration was notably enhanced in the CS-rGO group, with the TA-loaded formulation (CS-rGO-TA_3) further accelerating closure. Specifically, the CS-rGO-TA_3 hydrogel achieved over 60% closure in 24 hours and exceeded 90% by

36 hours. By 48 hours, complete closure was observed in both hydrogel-treated groups and the positive control, while the negative control remained at approximately 70%. These findings highlight the hydrogel's excellent cytocompatibility and pro-migratory properties, both of which are essential for effective wound healing. Furthermore, the results are consistent with previous studies, such as that of Nie *et al.* (2025), in which an L-hydroxyproline-conjugated chitosan hydrogel integrated with TA-loaded PF127 micelles promoted over 80% cell viability after 72 hours and significantly improved fibroblast migration, leading to better wound closure outcomes in *in vitro* models.[70]

3.5. Irritation potential

Materials intended for wound healing must demonstrate both biocompatibility and safety to prevent adverse reactions in dermal tissues. Sensitive skin models, such as Guinea pigs, offer valuable insight into the dermatological safety of hydrogel formulations before potential clinical application. In this study, the skin irritation potential of the CS-rGO-TA_3 hydrogel was evaluated (Fig. 2F). The results showed that CS-rGO-TA_3 did not induce any signs of irritation, with no visible changes observed upon removal of the hydrogel, resulting in an irritation index of 0.0 (Table S2). Furthermore, all animals maintained normal feeding and drinking behavior, exhibited unimpaired motor function, and showed no abnormal signs such as lethargy, restlessness, pruritus, or irritability. As no clinical symptoms were detected throughout the observation period, histopathological skin sampling was deemed unnecessary. These findings collectively support the excellent biocompatibility and dermatological safety of the CS-rGO-TA_3 hydrogel.

3.6. *In vivo* healing assay

Building upon our earlier *in vitro* findings that highlighted the potent antimicrobial properties and excellent biocompatibility of the CS-rGO-TA_3 hydrogel, we proceeded to evaluate its therapeutic efficacy in a rat model of full-thickness excisional wounds. All treatment groups exhibited significantly enhanced wound contraction compared to the untreated control, achieving over 20% wound closure as early as day 2 post-injury (Fig. 3A and B). This early response suggests a rapid onset of bioactivity, likely facilitated by the hydrogel's capacity to maintain a moist environment, control microbial load, and modulate the local inflammatory milieu. Among the groups, CS-rGO-TA_3-treated wounds displayed the greatest reduction in wound area and the fastest rate of closure, outperforming both the untreated control and hydrogels lacking TA (Fig. 3A and B). This superior performance is likely attributable to the combined effects of the hydrogel's physicochemical properties: effective exudate absorption, sustained hydration of the wound bed, and intimate contact with tissue surfaces, which together enhance antibacterial efficacy and attenuate inflammation. By day 7, wound closure rates had increased significantly across all treated groups. Specifically, the CS-rGO-TA_3 group achieved 65.15 ± 2.87% closure, compared to 60.06 ± 2.42% in the CS-rGO group, 55.94 ± 1.76% in the CS group, and 51.47 ± 2.87% in the untreated control (Fig. 3A). By day 14, wounds treated with the TA-loaded hydrogel were nearly fully re-epithelialized, accompanied by visible hair regrowth around the wound edges—a sign of dermal restoration.

Quantitative analysis confirmed statistically significant differences between groups, with CS-rGO-TA_3-treated wounds reaching 98.77 ± 0.69% closure, compared to 77.58 ± 1.21% in the untreated group (Fig. 3B). The enhanced healing observed in the CS-rGO-TA_3 group can be largely attributed to the astringent and bioactive properties of TA, which support faster wound contraction and re-epithelialization.[71] These results not only agree with previous studies but also expand upon them. Several studies have demonstrated that CS-polyphenol-based hydrogels induce progressive improvements in granulation tissue formation and moderate reductions in pro-inflammatory cytokines, promote hemostasis, stimulate angiogenesis, and exhibit significant antioxidant activity.[72] Taken together, these effects contribute to more organized healing and are particularly beneficial in complex or chronic wound settings, such as diabetic ulcers. Furthermore, rGO-reinforced systems are primarily associated with increased angiogenesis and more efficient collagen remodeling, effects attributable to improved mechanical stability, matrix structural integrity, and modulation of the cellular microenvironment.[73,74] Taken together, this background supports the idea that the simultaneous combination of TA and rGO within the CS matrix integrates complementary mechanisms—immunomodulation, oxidative control, and structural reinforcement—that explain the superior performance observed in the present study.

To gain deeper insight into tissue-level healing, histopathological analyses were conducted to evaluate the progression of wound regeneration following treatment. Hematoxylin and eosin (H&E) staining revealed progressive re-epithelialization across all treated groups, with the CS-rGO-TA_3 hydrogel displaying the most robust and organized epidermal regeneration (Fig. 3C). Wound contraction was evident beneath the newly formed epidermis, and by day 7, the presence of inflammatory infiltrates—including neutrophils, lymphocytes, and macrophages—confirmed active engagement of the inflammatory phase. These histological findings were consistent with molecular data from gene expression analysis, reinforcing the observed biological activity. Between days 7 and 14 post-injury, tissue sections from the treated groups demonstrated ongoing re-epithelialization, abundant granulation tissue formation, emerging hair follicles, and clear signs of neovascularization. A gradual reduction in inflammatory cell infiltration was observed over time, with the CS-rGO-TA_3 group displaying the lowest inflammatory scores by day 14, indicating a more rapid resolution of inflammation and an accelerated transition toward the proliferative phase of healing. Interestingly, the TA-treated group also showed a thinner, more compact epidermis at later stages, consistent with advanced tissue remodeling. This may be attributed to tannic acid's capacity to precipitate lipid–protein complexes and promote the formation of a flexible, protective scab that supports tissue stabilization and reduces further irritation.[75]

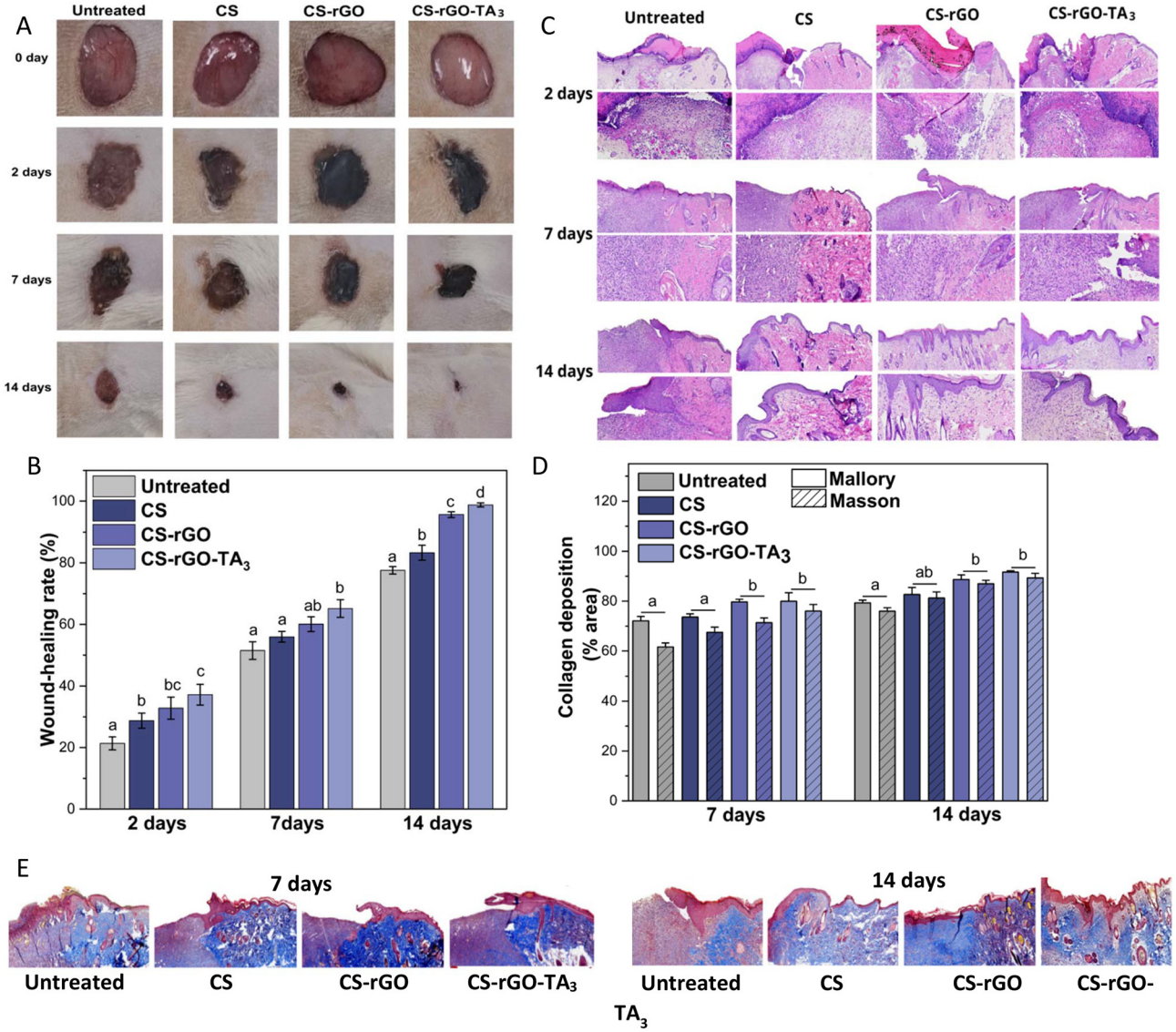

Fig. 3 Characterization of the synthesized materials in an *in vivo* model (rats). Images of wound evolution over time (A), wound closure rate (B), qualitative histological evaluation of the experimental groups using hematoxylin and eosin (H&E) staining at 600× and 100× magnification (C). Quantification of collagen deposition using Mallory staining and Masson's trichrome staining at 7 and 14 days (D). Images of Masson's trichrome staining at 600× magnification at 7 and 14 days (E). Results were expressed as mean ± standard error of the mean (significance levels were set at $p < 0.05$, and differences were considered significant when the groups compared displayed different letters).

3.7. Collagen deposition assay

Collagen deposition is critical for wound strength and dermal remodeling.[76] Quantitative analysis of collagen content, performed using Mallory and Masson's Trichrome staining alongside image analysis *via* ImageJ software (Fig. 3D and E), demonstrated a significant increase in collagen deposition in all treated groups compared to the untreated control. Notably, the CS-rGO-TA_3 hydrogel induced the highest levels of collagen accumulation at both 7 and 14 day post-injury. These effects were especially evident in the CS-rGO and CS-rGO-TA_3 groups, with the TA-enriched hydrogel showing the most substantial collagen density by day 14. These findings highlight the hydrogel's capacity to enhance extracellular matrix remodeling and restore tissue integrity. The observed increase in collagen content is likely influenced by the anti-inflammatory activity of tannic acid, which reduces oxidative and inflammatory damage while promoting a regenerative microenvironment.[77,78] In this context, the dual role of collagen types becomes relevant: type I collagen, the most abundant in mature skin, provides tensile strength and structural integrity, while type III collagen plays a regulatory role during early repair, facilitating matrix organization, cellular migration, and scar minimization.[79] Protein expression assays (Fig. 4A and B) revealed a predominance of type III collagen in the early stages of healing, followed by a progressive shift toward type I collagen as remodeling advanced, reflecting the physiological dynamics of

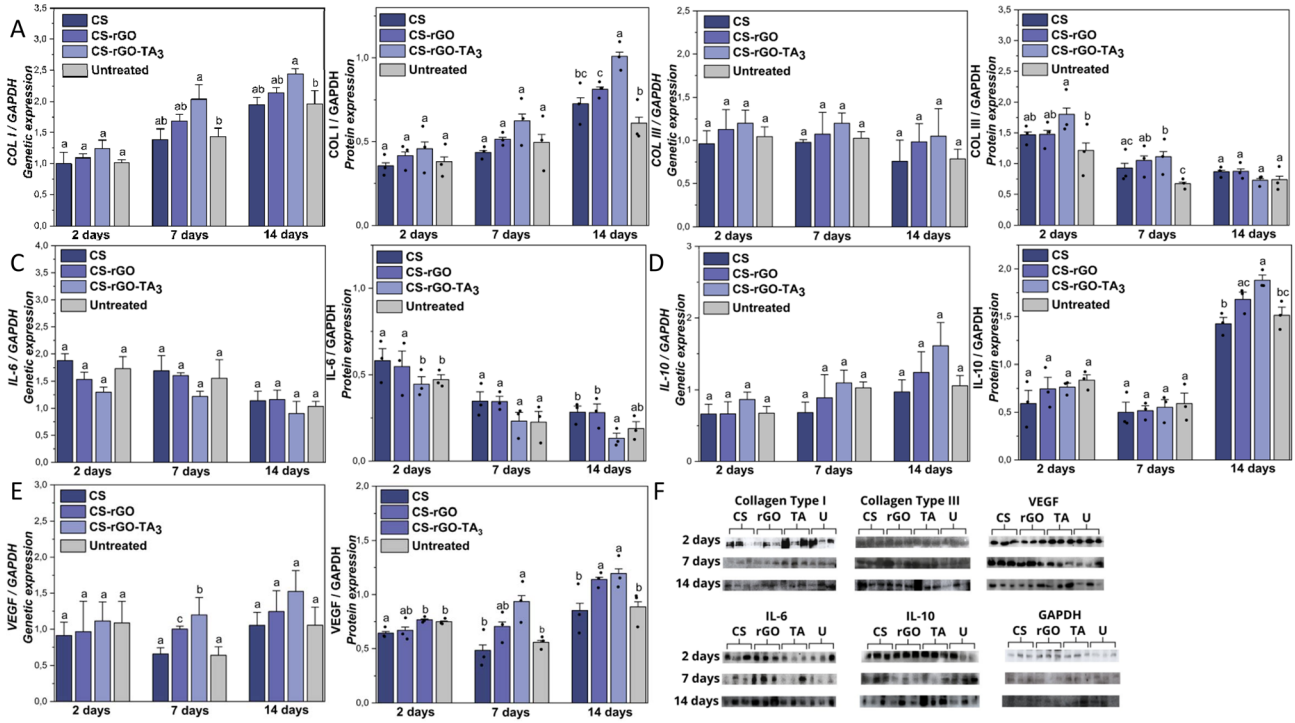

Fig. 4 Relative gene and protein expression at 2, 7 and 14 days. COL I (A), COL III (B), IL-6 (C), IL-10 (D) and VEGF (E). Protein expression bands by western blot analysis (F). Results were expressed as mean ± standard error of the mean (significance levels were set at $p < 0.05$, and differences were considered significant when the groups compared displayed different letters).

wound maturation.[80] Correspondingly, mRNA expression analysis confirmed the upregulation of both type I and III collagen transcripts during the proliferative phase, with the CS-rGO-TA_3 group exhibiting significantly higher expression levels than the untreated group (Fig. 4A and B). These effects may be further enhanced by the astringent nature of TA, which is believed to facilitate collagen fiber crosslinking, thereby improving the mechanical strength and structural organization of the extracellular matrix.[81]

3.8. Molecular analysis by western blot and RT-qPCR

The expression of interleukins following tissue injury plays a central role in regulating inflammation, orchestrating healing responses, and influencing scar formation.[82] Interleukin-10 (IL-10), a key anti-inflammatory cytokine, plays a crucial role in regulating the inflammatory phase of wound healing by limiting excessive immune activation and promoting tissue homeostasis. It suppresses excessive neutrophil and macrophage activation and downregulates the expression of proinflammatory cytokines such as interleukin-6 (IL-6).[83,84] In addition, IL-10 contributes to tissue repair by facilitating the recruitment of endothelial progenitor cells and promoting re-epithelialization, thereby supporting vascular regeneration and epidermal restoration.[85] As shown in Fig. 4C and D, both gene and protein expression levels of IL-6 were elevated during the early inflammatory phase (day 2), whereas IL-10 expression remained relatively low. This pattern is consistent with the physiological response to acute injury. However, as healing progressed into the proliferative phase (days 7 to 14), a reversal in expression trends was observed. Importantly, treatment with CS-rGO-TA_3 resulted in a pronounced reduction in IL-6 expression and a concomitant increase in IL-10 levels at both the transcriptional and protein levels, indicating effective modulation of the inflammatory response. These findings suggest that the TA-loaded hydrogel more effectively attenuated the inflammatory response, promoting an earlier transition toward tissue regeneration—an effect supported by existing literature on the anti-inflammatory properties of TA. Efficient resolution of inflammation is a prerequisite for the onset of the proliferative phase, during which granulation tissue forms and fibroblasts synthesize extracellular matrix components such as collagen. Collagen serves as a scaffold for cellular organization, enabling angiogenesis and epithelial coverage.[86] The gene and protein expression of type I collagen further supports this regenerative progression, with the CS-rGO-TA_3 hydrogel promoting significantly higher expression levels compared to other groups. These data highlight the critical link between controlled inflammation and enhanced matrix deposition.

Vascular endothelial growth factor (VEGF), a key regulator of angiogenesis, plays a pivotal role in wound healing by supporting vascular remodeling, re-epithelialization, and collagen synthesis.[87] As shown in Fig. 4E, VEGF expression was upregulated across all treatment groups during the regenerative phase, with the highest levels observed in the TA-loaded hydrogel group ($p < 0.05$). This enhanced VEGF activity likely con-

tributed to improved tissue perfusion and oxygenation, thereby alleviating metabolic stress within the wound microenvironment.[88–90] Collectively, these results underscore the diverse biological functions of tannins in modulating key phases of wound healing, from inflammation control to tissue regeneration. Beyond their well-established antioxidant and anti-inflammatory properties, TA have also been shown to stimulate fibroblast and keratinocyte proliferation, promote neovascularization, and facilitate wound contraction—critical processes that work synergistically to accelerate tissue regeneration and support functional skin repair.[91] The combined effect of these mechanisms, as demonstrated by the CS-rGO-TA_3 hydrogel, suggests its strong therapeutic potential in accelerating wound healing and improving overall tissue repair quality.

Myeloperoxidase (MPO) is a key enzyme produced by activated neutrophils, playing a central role in microbial clearance through the generation of reactive oxygen species (ROS).[92] At day 2 post-injury, all hydrogel-treated groups exhibited elevated MPO gene expression relative to the untreated control, although these differences did not reach statistical significance. As healing progressed, however, a significant reduction in MPO expression was observed in the CS-rGO-TA_3 group by day 14, compared to both the CS and untreated groups (Fig. 5A). Although MPO levels were also lower than those in the CS-rGO group, this difference was not statistically significant. These findings align with the enhanced wound closure and elevated type I collagen expression observed in the CS-rGO-TA_3 group, reinforcing its role in promoting effective tissue regeneration. Elevated MPO levels are often associated with prolonged inflammation and impaired healing, as excessive ROS production can damage surrounding tissues and delay the transition to the proliferative phase. The observed reduction in MPO expression at later time points suggests successful resolution of the inflammatory phase, likely following initial microbial control. This interpretation aligns with previous *in vivo* and *ex vivo* studies, which demonstrated that MPO can inhibit neutrophil adhesion and migration, and that the accumulation of hydrogen peroxide (H_2O_2), along with MPO released by infiltrating neutrophils, exacerbates oxidative stress and epithelial injury.[93]

Arginase 1 (ARG1), on the other hand, is a hallmark of reparative (M2) macrophage polarization and plays a crucial role in orchestrating wound healing. It modulates the inflammatory response, facilitates cell migration, supports restoration of the skin barrier, and contributes to tissue remodeling.[94,95] At day 2 post-wounding, ARG1 mRNA expression was upregulated in all treated groups compared to the control, with CS-rGO-TA_3 showing significantly higher levels (Fig. 5B). This trend persisted at days 7 and 14, where Arg1 expression remained elevated in all treatment groups, with the CS-rGO-TA_3 hydrogel consistently inducing the highest expression. These findings suggest a sustained pro-repair immune response in the CS-rGO-TA_3 group, supporting faster resolution of inflammation and enhanced tissue regeneration. This is further supported by previous reports highlighting the role of ARG1 in promoting collagen synthesis through the conversion of L-arginine into ornithine, a key precursor in collagen biosynthesis.[96] These results corroborate our findings on enhanced collagen expression in treated groups. The elevated ARG1 levels observed in our study correlate well with the enhanced collagen deposition documented

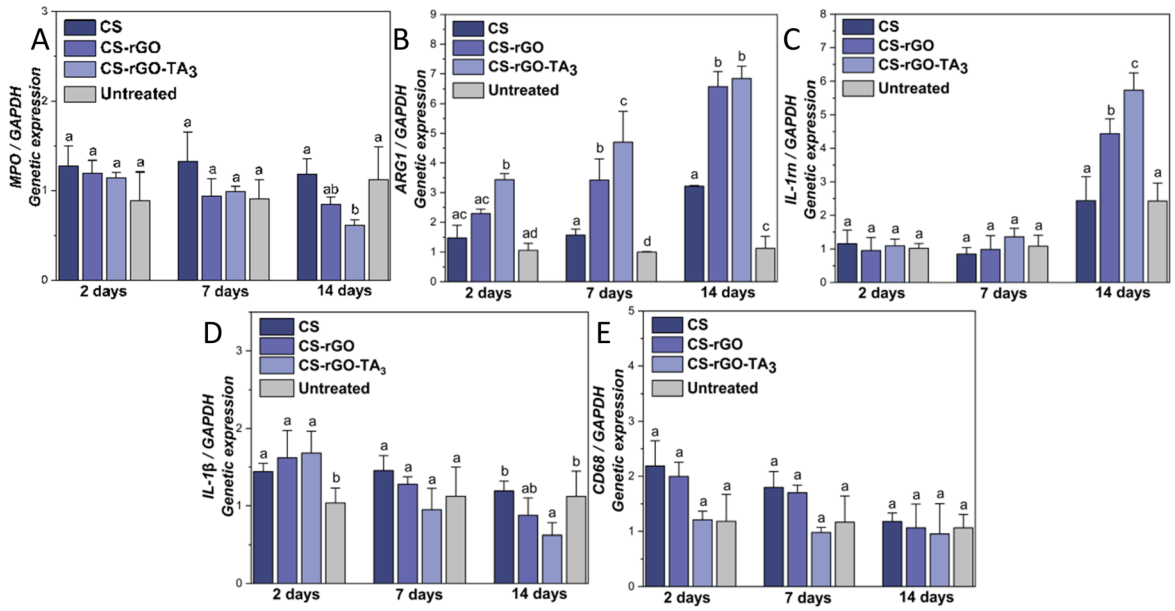

Fig. 5 Relative gene expressions at 2, 7 and 14 days. MPO (A), ARG1 (B), IL-1rn (C), IL-1β (D), and CD68 (E). Results were expressed as mean ± standard error of the mean (significance levels were set at $p < 0.05$, and differences were considered significant when the groups compared displayed different letters).

in histological and molecular analyses, further underscoring the regenerative capacity of the CS-rGO-TA_3 hydrogel.

A prolonged or dysregulated inflammatory response is a recognized barrier to effective wound healing, underscoring the critical role of tightly regulated proinflammatory cytokine activity in orchestrating successful tissue repair.[97] Among these, the interleukin-1 receptor antagonist (IL-1rn) plays a pivotal role in modulating the local inflammatory environment by suppressing IL-6 and IL-1β expression while promoting IL-10 production.[98] In our study, IL-1rn expression levels at days 2 and 7 post-injury showed no significant differences between the treated and control groups, suggesting that early anti-inflammatory signaling remained comparable across conditions during the initial phases of wound healing. However, at day 2, the untreated group exhibited markedly higher IL-1β expression compared to all treated groups, indicating a delayed resolution of inflammation, even in an acute wound model. By day 14, the CS-rGO-TA_3-treated group showed the highest IL-1rn expression and the lowest IL-1β levels across all groups (Fig. 5D and E), suggesting more efficient control of the inflammatory response. This observation is supported by prior studies indicating that IL-1 inhibition can attenuate proinflammatory cytokine production (*e.g.*, IL-1β, IL-6), reduce myofibroblast activity, and enhance anti-inflammatory cytokine release (*e.g.*, IL-10), as well as endothelial cell recruitment, M2 macrophage polarization, and granulation tissue formation—creating a transiently less inflammatory environment conducive to tissue repair.[99,100]

At 2 days post-injury, the CD68 expression marker of macrophage infiltration was significantly elevated in the CS and CS-rGO groups compared to the CS-rGO-TA_3 and untreated groups, indicating a more intense early inflammatory response (Fig. 5E). This pattern is characteristic of the early inflammatory phase, during which macrophage recruitment plays a pivotal role in clearing cellular debris and defending against potential pathogens. By day 7, CD68 expression had declined across all groups, with the CS-rGO-TA_3 group showing the lowest levels, suggesting a more rapid resolution of macrophage-mediated inflammation. This is notable given that prolonged persistence of proinflammatory macrophages is associated with delayed healing, chronic inflammation, and fibrosis.[101,102] By day 14, CD68 expression had normalized across all groups, reflecting progression into the proliferative and remodeling phases of wound repair. This temporal pattern aligns with well-established dynamics of macrophage infiltration, where a decrease in inflammatory cell presence coincides with the onset of tissue regeneration and extracellular matrix remodeling.[103] These findings are consistent with previously reported expression patterns of both pro- and anti-inflammatory markers (IL-6, IL-1β, IL-10, IL-1rn, Arg1), as well as with the accelerated wound healing observed in the CS-rGO-TA_3 group. The sustained reduction in macrophage activity in this group aligns with known anti-inflammatory effects of polyphenolic compounds, which have been shown to promote macrophage polarization toward the M2 reparative phenotype.[104,105] This immunomodulatory shift supports the hypothesis that TA-enriched hydrogels facilitate the transition from inflammation to regeneration, thereby enhancing the wound healing process. Moreover, the improved outcomes observed in collagen deposition, neovascularization, and overall wound closure in the CS-rGO-TA_3 group are likely downstream effects of this early and effective modulation of the inflammatory response. These results are consistent with previous studies highlighting the therapeutic potential of TA and other natural anti-inflammatory agents in promoting cutaneous repair through immune regulation and support of the proliferative phase.[106] Although TA are the main contributors to the observed anti-inflammatory response, rGO may also actively participate in immunomodulation.[107,108] Previous studies have shown that rGO can inhibit pro-inflammatory cytokines and influence macrophage phenotype, while stabilizing polyphenols and modulating their release.[109–112] In our system, rGO likely contributes both structurally and biologically, complementing the immunomodulatory action of TA.

The results obtained in this study demonstrate that the CS-rGO-TA_3 hydrogel significantly accelerates wound closure (98.77 ± 0.69% by day 14), along with more efficient re-epithelialization, greater organization of collagen fibers, and marked modulation of the inflammatory profile (↓IL-6, ↓IL-1β, ↑IL-10, ↑Arg1). In comparison with previously reported systems, the CS-rGO-TA_3 hydrogel demonstrates enhanced wound closure and immunomodulatory effects. This performance is comparable to or even superior to that reported for systems based solely on CS-polyphenols or CS/rGO compounds. For example, Li *et al.* (2023) reported that a polyphenol-loaded CS hydrogel achieved approximately 85–90% closure by day 14 in a murine model, with a significant reduction in IL-6 but without in-depth assessment of macrophage polarization.[68] Similarly, Sun *et al.* (2024) described a CS-polyphenol system that improved granulation tissue formation and reduced inflammatory markers, achieving close to 90% closure at 14 days in acute wounds.[113] In the case of hydrogels reinforced with graphene derivatives, Graça *et al.* (2022) reported that a CS/rGO system promoted greater angiogenesis and collagen organization, with closure rates close to 88–92% at day 14, mainly attributed to structural reinforcement and improvement of the moist microenvironment.[25] Likewise, Elhami *et al.* (2024) showed that CS-graphene compounds improved mechanical stability and antimicrobial control, achieving approximately 90% closure.[114] In comparison, the CS-rGO-TA_3 system not only achieves a higher closure percentage (≈98.8% by day 14), but also demonstrates a more comprehensive regulation of the inflammatory process, evidenced by the coordinated decrease in IL-6 and IL-1β and the increase in IL-10 and Arg1, suggesting a more efficient transition to a reparative macrophage phenotype. This more complete immunomodulation is not always reported in CS-polyphenol or CS/rGO systems alone. In this sense, our results support the hypothesis of a synergistic effect derived from the combination of TA (antioxidant and immunomodulatory activity) and rGO (mechanical reinforcement and structural stabilization) within the CS matrix, which promotes faster, more organized healing with

early inflammatory resolution. However, these results should be interpreted with caution, as differences in experimental models, wound size, and evaluation methods may limit direct comparison across studies. Despite these promising results, several limitations should be acknowledged. First, while the TA release profile was sufficient to induce early biological effects, further optimization of the long-term release kinetics may be necessary for more widespread clinical applications. Additionally, while the observed biological effects are promising, the contribution of each component (CS, rGO, and TA) cannot be fully decoupled within the current experimental design. Second, slight variations in the physicochemical characteristics of rGO (*e.g.*, degree of reduction and lateral size) could influence reproducibility and bioactivity. The antibacterial activity, although significant, remains within moderate log-reduction ranges, suggesting that further optimization may be required for applications involving highly infected wounds. Finally, the acute murine wound model used in this study does not fully replicate the complexity of chronic human wounds. Furthermore, the acute murine wound model used does not fully reproduce the complexity of chronic or infected human wounds, which may involve impaired angiogenesis, persistent inflammation, and biofilm formation. Future studies should therefore include long-term release evaluation, standardized rGO characterization, and validation in clinically relevant wound models.

4. Conclusions

The CS-rGO-TA_3 hydrogel demonstrated a controlled and sustained release of TA, attributed to its dense network structure, which also contributed to its superior antioxidant activity by effectively eliminating free radicals. In addition to these properties, CS-rGO-TA_3 exhibited excellent antibacterial activity against *E. coli* and *S. aureus*, along with remarkable biocompatibility, evidenced by high viability of human dermal fibroblasts and the absence of toxicity or irritation. Furthermore, this hydrogel promoted cell migration and the organized deposition of type I and III collagen, facilitating tissue regeneration. In animal models, treatment with CS-rGO-TA_3 significantly accelerated wound healing, reduced inflammation, and facilitated the formation of a flexible scab, contributing to a faster and structurally robust recovery. The presence of TA in the formulation modulated the inflammatory response by decreasing proinflammatory cytokines (IL-6, IL-1β) and enhancing anti-inflammatory cytokines (IL-10, IL-1rn), thereby promoting an early transition from the inflammatory to the proliferative phase. This immunomodulation was reflected in controlled macrophage infiltration, with reduced expression of proinflammatory markers such as CD68 and MPO, alongside sustained upregulation of ARG1, associated with polarization toward reparative M2 macrophage phenotypes. The molecular effects translated into functional improvements, including enhanced angiogenesis, efficient cell migration, and accelerated granulation tissue formation, resulting in a higher wound rate compared to controls. Collectively, these findings position the CS-rGO-TA_3 hydrogel as a safe and effective therapeutic strategy for cutaneous repair, particularly in wounds with impaired or chronic healing, by creating a favorable microenvironment that accelerates tissue regeneration and improves the quality of the repaired tissue.

Author contributions

Isleidy Ruíz: conceptualization; data curation; formal analysis; funding acquisition; investigation; methodology; software; validation; writing – original draft. Luisbel González: data curation; investigation. Julia Schneider: data curation; investigation. Cintia Sena: data curation; investigation. Maria E. C. do Amaral: conceptualization; formal analysis; investigation. Guilherme Ferreira: conceptualization; formal analysis; funding acquisition; investigation; project administration; resources; supervision; writing – review & editing. Katherina Fernández: conceptualization; formal analysis; funding acquisition; investigation; project administration; resources; supervision; writing – review & editing.

Conflicts of interest

There are no conflicts to declare.

Data availability

Data will be made available on request.

Supplementary information (SI) is available. See DOI: https://doi.org/10.1039/d5bm01612f.

Acknowledgements

We gratefully acknowledge the financial support provided by the FONDECYT-Chile Project No. 1210770 and the United Nations University Program for Biotechnology in Latin America and the Caribbean (UNU-BIOLAC), which made this research possible. Isleidy Ruíz thanks the National Research and Development Agency (ANID) for the Doctorate in Chemical Engineering (UdeC) scholarship ANID-PFCHA/National Doctorate 21210191. Finally, the authors acknowledge assistance in the Center for Advanced Microscopy for the SEM (University of Concepción).

References

1 Y. Liang, J. He and B. Guo, *ACS Nano*, 2021, **15**, 12687–12722, DOI: 10.1021/acsnano.1c04206.
2 V. Gounden and M. Singh, *Gels*, 2024, **10**, 1–21, DOI: 10.3390/gels10010043.

3 X. Zhao, H. Wu, B. Guo, R. Dong and Y. Qiu, *Biomaterials*, 2017, **122**, 34–47, DOI: 10.1016/j.biomaterials.2017.01.011.
4 G. Chen, F. Wang, X. Zhang, Y. Shang and Y. Zhao, *Sci. Adv.*, 2023, **9**, 1–10, DOI: 10.1126/sciadv.adg3478.
5 N. Asadi, H. Pazoki-Toroudi, A. R. Del Bakhshayesh, A. Akbarzadeh, S. Davaran and N. Annabi, *Int. J. Biol. Macromol.*, 2021, **170**, 728–750, DOI: 10.1016/j.ijbiomac.2020.12.202.
6 I. Ruiz, S. Castro, V. Aedo, M. Tapia, L. González, C. Aguayo and K. Fernández, *ChemistrySelect*, 2024, **9**, 1–10, DOI: 10.1002/slct.202402444.
7 F. Fan, S. Saha and D. Hanjaya-Putra, *Front. Bioeng. Biotechnol.*, 2021, **9**, 1–24, DOI: 10.3389/fbioe.2021.718377.
8 H. Chen, J. Cheng, L. Ran, K. Yu, B. Lu, G. Lan, F. Dai and F. Lu, *Carbohydr. Polym.*, 2018, **201**, 522–531, DOI: 10.1016/j.carbpol.2018.08.090.
9 J. Xiang, L. Shen and Y. Hong, *Eur. Polym. J.*, 2020, **130**, 1–13, DOI: 10.1016/j.eurpolymj.2020.109609.
10 Z. Yang, R. Huang, B. Zheng, W. Guo, C. Li, W. He, Y. Wei, Y. Du, H. Wang, D. Wu and H. Wang, *Adv. Sci.*, 2021, **8**, 1–12, DOI: 10.1002/advs.202003627.
11 I. Bano, M. Arshad, T. Yasin, M. Ghauri and M. Younus, *Int. J. Biol. Macromol.*, 2017, **102**, 380–383, DOI: 10.1016/j.ijbiomac.2017.04.047.
12 A. Moeini, P. Pedram, P. Makvandi, M. Malinconico and G. d'Ayala, *Carbohydr. Polym.*, 2020, **233**, 1–16, DOI: 10.1016/j.carbpol.2020.115839.
13 H. Liu, C. Wang, C. Li, Y. Qin, Z. Wang, F. Yang, Z. Li and J. Wang, *RSC Adv.*, 2018, **8**, 7533–7549, DOI: 10.1039/C7RA13510F.
14 Y. Gutha, J. Pathak, W. Zhang, Y. Zhang and X. Jiao, *Int. J. Biol. Macromol.*, 2017, **103**, 234–241, DOI: 10.1016/j.ijbiomac.2017.05.020.
15 M. Abbas, T. Hussain, M. Arshad, A. R. Ansari, A. Irshad, J. Nisar, F. Hussain, N. Masood, A. Nazir and M. Iqbal, *Int. J. Biol. Macromol.*, 2019, **164**, 2726–2744, DOI: 10.1016/j.ijbiomac.2020.08.153.
16 M. Matica, F. Aachmann, A. Tøndervik, H. Sletta and V. Ostafe, *Int. J. Mol. Sci.*, 2019, **20**, 1–33, DOI: 10.3390/ijms20235889.
17 Q. Bai, Q. Gao, F. Hu, C. Zheng, W. Chen, N. Sun, J. Liu, Y. Zhang, X. Wu and T. Lu, *Int. J. Biol. Macromol.*, 2023, **232**, 123271, DOI: 10.1016/j.ijbiomac.2023.123271.
18 M. Dumont, R. Villet, M. Guirand, A. Montembault, T. Delair, S. Lack, M. Barikosky, A. Crepet, P. Alcouffe, F. Laurent and L. David, *Carbohydr. Polym.*, 2018, **190**, 31–42, DOI: 10.1016/j.carbpol.2017.11.088.
19 A. Li, M. Bin, S. Hua, R. Ping, L. Ding, B. Tian and X. Zhang, *Carbohydr. Polym.*, 2024, **333**, 1–17, DOI: 10.1016/j.carbpol.2024.121952.
20 N. Bellier, P. Baipaywad, N. Ryu, J. Y. Lee and H. Park, *BioMed Central Ltd*, 2022, **26**, 1–23, DOI: 10.1186/s40824-022-00313-2.
21 L. González, V. Espinoza, M. Tapia, V. Aedo, I. Ruiz, M. Meléndrez, C. Aguayo, L. I. Atanase and K. Fernández, *Gels*, 2024, **10**, 448–464, DOI: 10.3390/gels10070448.
22 E. A. Chiticaru and M. Ionita, *FlatChem*, 2022, **35**, 100417, DOI: 10.1016/j.flatc.2022.100417.
23 O. Cebadero-Domínguez, B. Ferrández-Gómez, S. Sánchez-Ballester, J. Moreno, A. Jos and A. M. Cameán, *Toxicol. Rep.*, 2022, **9**, 1130–1138, DOI: 10.1016/j.toxrep.2022.05.010.
24 D. Jiao, A. Zheng, Y. Liu, X. Zhang, X. Wang, J. Wu, W. She, K. Lv, L. Cao and X. Jiang, *Bioact. Mater.*, 2021, **6**, 2011–2028, DOI: 10.1016/j.bioactmat.2020.12.003.
25 M. Graça, B. Melo, R. Lima-Sousa, P. Ferreira, A. Moreira and I. Correia, *Int. J. Biol. Macromol.*, 2022, **229**, 224–235, DOI: 10.1016/j.ijbiomac.2022.12.291.
26 Z. Xu, S. Han, Z. Gu and J. Wu, *Adv. Healthcare Mater.*, 2020, **9**, 1–11, DOI: 10.1016/adhm.201901502.
27 I. Stefanov, S. Pérez-Rafael, J. Hoyo, J. Cailloux, O. O. Santana Pérez, D. Hinojosa-Caballero and T. Tzanov, *Biomacromolecules*, 2017, **18**, 1544–1555, DOI: 10.1016/acs.biomac.7b00111.
28 I. Guimarães, S. Baptista-Silva, M. Pintado and A. L. Oliveira, *Appl. Sci.*, 2021, **11**, 1230–1250, DOI: 10.3390/app11031230.
29 G. Rocasalbas Lozano, *Development of multifunctional biopolymeric materials for teatment of decubitus ulcers*, Universitat Politècnica de Catalunya, 2012, https://dialnet.unirioja.es/servlet/tesis?codigo=95520.
30 M. C. Jacques, T. T. Andrighetti, C. Schmitt, C. M. D. De Freitas, C. F. De Barros, A. S. Antunes, É. J. Bunhak and I. A. De Lima, *Braz. J. Health Rev.*, 2023, **6**, 29548–29566, DOI: 10.34119/bjhrv6n6-230.
31 S. Carrasco, L. González, M. Tapia, B. F. Urbano, C. Aguayo and K. Fernández, *Polymers*, 2024, **16**, 1081–1098, DOI: 10.3390/polym16081081.
32 J. V. Helaehil, L. V. Helaehil, L. F. Alves, B. Huang, M. Santamaria-Jr, P. Bartolo and G. F. Caetano, *Bioengineering*, 2023, **10**, 75–90, DOI: 10.3390/bioengineering10010075.
33 W. Feng and Z. Wang, *iScience*, 2022, **25**, 103629, DOI: 10.1016/J.ISCI.2021.103629.
34 L. González, B. Zapata, T. Figueroa, I. Ruiz, L. F. Montoya, E. J. Pino, C. Aguayo, J. R. Toledo, A. Romero and K. Fernández, *Int. J. Biol. Macromol.*, 2025, **311**, 144082, DOI: 10.1016/J.IJBIOMAC.2025.144082.
35 X. Qiu, Y. Shen, R. Yang, H. Zhang and S. Zhao, *Environ. Technol.*, 2019, **40**, 202–209, DOI: 10.1080/09593330.2027.1384072.
36 L. Wang, X. Chen, X. Xi, S. H. Lee, W. C. Lum, Y. Huang, G. Du, X. Zhou and J. Zhang, *Int. J. Biol. Macromol.*, 2024, **282**, 1–32, DOI: 10.1016/j.ijbiomac.2024.137438.
37 K. Kosowska, P. Domalik-Pyzik, M. Krok-Borkowicz and J. Chłopek, *Materials*, 2019, **12**, 1–13, DOI: 10.3390/ma12132077.
38 R. Xue, L. He, J. Wu, X. Kong, Q. Wang, Y. Chi, J. Liu, Z. Wang, K. Zeng, W. Chen, H. Ren and B. Han, *Int. J. Biol. Macromol.*, 2024, **275**, 133303, DOI: 10.1016/j.ijbiomac.2024.133303.
39 J. Ahmed, M. Mulla and M. Maniruzzaman, *ACS Biomater. Sci. Eng.*, 2020, **6**, 88–99, DOI: 10.1021/acsbiomaterials.9b00201.

40 A. Biswal, S. S. Purohit, L. Mishra, M. Mishra, B. R. Routray, S. B. Biswal, S. Nayak, B. C. Behera and S. K. Swain, *Int. J. Biol. Macromol.*, 2025, **307**, 142057, DOI: 10.1016/j.ijbiomac.2025.142057.
41 H. Li, Y. Wang, Y. Kang, Y. He, J. Nie, C. Ma, X. Yang, Z. Chen and C. Lu, *Int. J. Biol. Macromol.*, 2025, **306**, 141259, DOI: 10.1016/j.ijbiomac.2025.141259.
42 Y. Tang, L. Zhang, X. Ge, Y. Zhang, Y. Liu and J. Wang, *Sep. Purif. Technol.*, 2024, **339**, 126618, DOI: 10.1016/j.seppur.2024.126618.
43 I. Kaminska, M. R. Das, Y. Coffinier, J. Niedziolka-Jonsson, J. Sobczak, P. Woisel, J. Lyskawa, M. Opallo, R. Boukherroub and S. Szunerits, *ACS Appl. Mater. Interfaces*, 2012, **4**, 1016–1020, DOI: 10.1021/am201664n.
44 F. Luo, K. Wu, J. Shi, X. Du, X. Li, L. Yang and M. Lu, *J. Mater. Chem. A*, 2017, **5**, 18542–18550, DOI: 10.1039/C7TA04740A.
45 K. Fernández, A. Llanquileo, M. Bustos, V. Aedo, I. Ruiz, S. Carrasco, M. Tapia, M. Pereira, M. F. Meléndrez, C. Aguayo and L. I. Atanase, *Polymers*, 2023, **15**, 2752–2770, DOI: 10.3390/polym15122752.
46 M. M. Al-Rajabi and Y. H. Teow, *Sustainable Chem. Pharm.*, 2023, **31**, 100939, DOI: 10.1016/j.scp.2022.100939.
47 T.-Y. Wu, C.-C. Huang, H.-C. Tsai, T.-K. Lin, P.-Y. Chen, H. F. Darge, Z.-X. Hong, H.-J. Harn, S.-Z. Lin, J.-Y. Lai and Y.-S. Chen, *Biomater. Adv.*, 2024, **156**, 213722, DOI: 10.1016/j.bioadv.2023.213722.
48 I. Ruíz, L. González, A. Quiroz, C. Aguayo, J. Toledo and K. Fernández, *ChemistrySelect*, 2025, **10**, DOI: 10.1002/slct.202502598.
49 X. Jing, H. Y. Mi, B. N. Napiwocki, X. F. Peng and L. S. Turng, *Carbon*, 2017, **125**, 557–570, DOI: 10.1016/J.CARBON.2017.09.071.
50 N. Li, Q. Ma, L. Xu, Y. Wang, L. Zhang, Y. Jiang and H. Liu, *Mater. Today Commun.*, 2024, **39**, 1–13, DOI: 10.1016/j.mtcomm.2024.109319.
51 M. F. P. Graça, B. L. Melo, R. Lima-Sousa, P. Ferreira, A. F. Moreira and I. J. Correia, *Int. J. Biol. Macromol.*, 2023, **229**, 224–235, DOI: 10.1016/J.IJBIOMAC.2022.12.291.
52 J. Nath, A. Chowdhury and S. K. Dolui, *Adv. Polym. Technol.*, 2018, **37**, 3665–3679, DOI: 10.1002/adv.22151.
53 C. Li, F. Li, K. Wang, Q. Wang, H. Liu, X. Sun and D. Xie, *Inorg. Chem. Commun.*, 2023, **155**, 110965, DOI: 10.1016/J.INOCHE.2023.110965.
54 İ. Kaya, B. Ayten and A. Ö. Yaşar, *React. Funct. Polym.*, 2020, **154**, 104667, DOI: 10.1016/J.REACTFUNCTPOLYM.2020.104667.
55 X. Xu, S. Deng, H. Essawy, S. H. Lee, W. C. Lum, X. Zhou, G. Du and J. Zhang, *Int. J. Biol. Macromol.*, 2024, **277**, 133784, DOI: 10.1016/J.IJBIOMAC.2024.133784.
56 J. Wang, G. Zhao, L. Jing, X. Peng and Y. Li, *Biochem. Eng. J.*, 2015, **98**, 75–83, DOI: 10.1016/j.bej.2014.11.013.
57 J. Xie, D. Jin, J. Qiu, J. Cui, M. Yin and X. Qu, *J. Mater. Chem. B*, 2022, **10**, 795–805, DOI: 10.1039/d1tb02101j.
58 X. He, X. Liu, J. Yang, H. Du, N. Chai, Z. Sha, M. Geng, X. Zhou and C. He, *Carbohydr. Polym.*, 2020, **247**, 1–12, DOI: 10.1016/j.carbpol.2020.116689.
59 N. Salimiyan, M. Gholami and R. Sedghi, *Chem. Eng. J.*, 2023, **471**, 144648, DOI: 10.1016/j.cej.2023.144648.
60 N. Micale, A. Citarella, M. S. Molonia, A. Speciale, F. Cimino, A. Saija and M. Cristani, *Molecules*, 2020, **25**, 1–33, DOI: 10.3390/molecules25143254.
61 J. Borges-Vilches, I. Unalan, C. R. Aguayo, K. Fernández and A. R. Boccaccini, *Biomacromolecules*, 2023, **24**, 5183–5193, DOI: 10.1021/acs.biomac.3c00727.
62 L. González, I. Ruiz, M. Raposo, C. Aguayo, J. R. Toledo, V. M. Perez-Puyana, A. Romero and K. Fernández, *Colloids Surf., B*, 2026, **257**, 115176, DOI: 10.1016/j.colsurfb.2025.115176.
63 A. Smeriglio, D. Barreca, E. Bellocco and D. Trombetta, *Br. J. Pharmacol.*, 2017, **174**, 1244–1262, DOI: 10.1111/bph.13630.
64 C. L. Ke, F. S. Deng, C. Y. Chuang and C. H. Lin, *Polymers*, 2021, **13**, 904–924, DOI: 10.3390/polym13060904.
65 X. Guo and N. Mei, *J. Food Drug Anal.*, 2014, **22**, 105–115, DOI: 10.1016/j.jfda.2014.01.009.
66 K. Fernández, A. Llanquileo, M. Bustos, V. Aedo, I. Ruiz, S. Carrasco, M. Tapia, M. Pereira, M. F. Meléndrez, C. Aguayo and L. I. Atanase, *Polymers*, 2023, **15**, 1–18, DOI: 10.3390/polym15122752.
67 L. Zuo, X. Wang, X. Cao, B. Chen, M. Shao, G. Yang, S. Fu and L. Wang, *J. Mech. Behav. Biomed. Mater.*, 2023, **145**, 105942, DOI: 10.1016/j.jmbbm.2023.105942.
68 D. Li, X. Dong, X. Liu, H. Lin, D. Yang, X. Shi, C. Chen, F. Tao, L. Jiang and H. Deng, *Carbohydr. Polym.*, 2024, **329**, 1–14, DOI: 10.1016/j.carbpol.2023.121687.
69 X. Su, X. Liu, S. Wang, B. Li, T. Pan, D. Liu, F. Wang, Y. Diao and K. Li, *Burns*, 2017, **43**, 830–838, DOI: 10.1016/j.burns.2016.10.010.
70 L. Nie, X. Ding, Y. Zhao, P. Ding, M. Zhao, Y. Sun, Y. Sun and G. Jiang, *Int. J. Biol. Macromol.*, 2025, **333**, 148767, DOI: 10.1016/j.ijbiomac.2025.148767.
71 L. Hernandes, L. Marques, S. Pereira, F. Palazzo, J. Carlos and P. De Mello, *Evol*, 2010, **46**, 431–437, DOI: 10.1590/S1984-82502010000300005.
72 Y. Song, L. Xing, X. Zou, C. Zhang, Z. Huang, W. Liu and J. Wang, *Int. J. Biol. Macromol.*, 2024, **258**, 128861, DOI: 10.1016/j.ijbiomac.2023.128861.
73 S. Mukherjee, P. Sriram, A. K. Barui, S. K. Nethi, V. Veeriah, S. Chatterjee, K. I. Suresh and C. R. Patra, *Adv. Healthcare Mater.*, 2015, **4**, 1722–1732, DOI: 10.1002/adhm.201500155.
74 Z. Li, S. Xiang, Z. Lin, E. N. Li, H. Yagi, G. Cao, L. Yocum, L. Li, T. Hao, K. K. Bruce, M. R. Fritch, H. Hu, B. Wang, P. G. Alexander, K. A. Khor, R. S. Tuan and H. Lin, *Biomaterials*, 2021, **277**, 1–15, DOI: 10.1016/j.biomaterials.2021.121082.
75 S. C. G. Pinto, F. G. Bueno, G. P. Panizzon, G. Morais, P. V. P. Dos Santos, M. L. Baesso, E. V. De Souza Leite-Mello and J. C. P. De Mello, *Planta Med.*, 2015, **81**, 1090–1096, DOI: 10.1055/s-0035-1546209.

76 L. Li, Y. Ma, G. He, S. Ma, Y. Wang and Y. Sun, *Biomed. Pharmacother.*, 2023, **161**, 114510, DOI: 10.1016/j.biopha.2023.114510.
77 T. Kumar, R. Malik and S. Zahrah Maqbool, *World J. Pharm. Pharm. Sci.*, 2015, **12**, 333, https://www.wjpps.com.
78 S. Vitale, S. Colanero, M. Placidi, G. Di Emidio, C. Tatone, F. Amicarelli and A. M. D'Alessandro, *Molecules*, 2022, **27**, 1–30, DOI: 10.3390/molecules27113566.
79 S. S. Mathew-Steiner, S. Roy and C. K. Sen, *Bioengineering*, 2021, **27**, 3566–3581, DOI: 10.3390/bioengineering8050063.
80 J. R. Merkel, B. R. DiPaolo, G. G. Hallock and D. C. Rice, *Proc. Soc. Exp. Biol. Med.*, 1988, **187**, 493–497, DOI: 10.3181/00379727-187-42694.
81 D. F. Rodrigues, F. F. Mendes, L. B. Menezes, W. L. Carvalho, S. Sá, J. A. Silva, L. A. Souza and L. A. F. Silva, *SCielo*, 2017, **69**, 1243–1250, DOI: 10.1590/1678-4162-9301.
82 I. Arranz-Valsero, L. Soriano-Romaní, L. García-Posadas, A. López-García and Y. Diebold, *Exp. Eye Res.*, 2014, **125**, 183–192, DOI: 10.1016/j.exer.2014.06.012.
83 Y. Sato, T. Ohshima and T. Kondo, *Biochem. Biophys. Res. Commun.*, 1999, **265**, 194–199, DOI: 10.1006/bbrc.1999.1455.
84 T. N. Y. Shen, S. Kanazawa, M. Kado, K. Okada, L. Luo, A. Hayashi, H. Mizuno and R. Tanaka, *PLoS One*, 2017, **12**, 1–19, DOI: 10.1371/journal.pone.0178232.
85 W. D. Short, E. Steen, A. Kaul, X. Wang, O. O. Olutoye, H. V. Vangapandu, N. Templeman, A. J. Blum, C. M. Moles, D. A. Narmoneva, T. M. Crombleholme, M. J. Butte, P. L. Bollyky, S. G. Keswani and S. Balaji, *FASEB J.*, 2022, **36**, 1–20, DOI: 10.1096/fj.201901024RR.
86 L. Vaidyanathan, *Biomed. Pharmacol. J.*, 2021, **14**, 1469–1480, DOI: 10.13005/bpj/2249.
87 P. Bao, A. Kodra, M. Tomic-Canic, M. S. Golinko, H. P. Ehrlich and H. Brem, *J. Surg. Res.*, 2009, **153**, 347–358, DOI: 10.1016/j.jss.2008.04.023.
88 F. Liu, X. Xu and T. Sun, *Diabetic Med.*, 2024, **41**, 1–10, DOI: 10.1111/dme.15388.
89 J. Hwang, K. L. Kiick and M. O. Sullivan, *ACS Appl. Mater. Interfaces*, 2023, **15**, 16434–16447, DOI: 10.21/acsami.2c23022.
90 F. Shams, H. Moravvej, S. Hosseinzadeh, E. Mostafavi, H. Bayat, B. Kazemi, M. Bandehpour, E. Rostami, A. Rahimpour and H. Moosavian, *Sci. Rep.*, 2022, **12**, 1–15, DOI: 10.1038/s41598-022-23304-8.
91 G. C. Lopes, A. C. C. Sanches, C. V. Nakamura, B. P. Dias Filho, L. Hernandes and J. C. P. de Mello, *J. Ethnopharmacol.*, 2005, **99**, 265–272, DOI: 10.1016/j.jep.2005.02.019.
92 V. Butin-Israeli, T. M. Bui, H. L. Wiesolek, L. Mascarenhas, J. J. Lee, L. C. Mehl, K. R. Knutson, S. A. Adam, R. D. Goldman, A. Beyder, L. Wiesmuller, S. B. Hanauer and R. Sumagin, *J. Clin. Invest.*, 2019, **129**, 712–726, DOI: 10.1172/jci122085.
93 T. W. Slater, A. Finkielsztein, L. A. Mascarenhas, L. C. Mehl, V. Butin-Israeli and R. Sumagin, *J. Immunol.*, 2017, **198**, 2886–2897, DOI: 10.4049/jimmunol.1601810.
94 J. M. Dzik, *Front. Immunol.*, 2014, **5**, 1–11, DOI: 10.3389/fimmu.2014.00544.
95 K. Paduch, A. Debus, B. Rai, U. Schleicher and C. Bogdan, *J. Immunol.*, 2019, **202**, 1453–1464, DOI: 10.4049/jimmunol.1801249.
96 R. A. Crompton, H. Williams, L. Campbell, L. H. Kheng, C. Saville, D. M. Ansell, A. Reid, J. Wong, L. A. Vardy, M. J. Hardman and S. M. Cruickshank, *J. Invest. Dermatol.*, 2022, **142**, 1206–1216, DOI: 10.1016/j.jid.2021.09.009.
97 C. Yan, N. Gao, H. Sun, J. Yin, P. Lee, L. Zhou, X. Fan and F.-S. Yu, *Am. J. Pathol.*, 2016, **186**, 1466–1480, DOI: 10.1016/j.ajpath.2016.01.019.
98 C. S. Chamberlain, E. M. Leiferman, K. E. Frisch, S. L. Brickson, W. L. Murphy, G. S. Baer and R. Vanderby, *PLoS One*, 2013, **8**, 1–12, DOI: 10.1371/journal.pone.0071631.
99 D. P. Perrault, A. Bramos, X. Xu, S. Shi and A. K. Wong, *Ann. Plast. Surg.*, 2018, **80**, S317–S321, DOI: 10.1097/sap.0000000000001417.
100 E. A. Nicolli, A. Ghosh, S. Haft, R. Frank, C. J. Saunders, N. Cohen and N. Mirza, *Ann. Otol., Rhinol., Laryngol.*, 2015, **125**, 284–289, DOI: 10.1177/0003489415610588.
101 P. J. Murray and T. A. Wynn, *Nat. Rev. Immunol.*, 2011, **11**, 723–737, DOI: 10.1038/nri3073.
102 J. Qian, E. Lu, H. Xiang, P. Ding, Z. Wang, Z. Lin, B. Pan, C. Zhang and Z. Zhao, *J. Nanobiotechnol.*, 2024, **22**, 550, DOI: 10.1186/s12951-024-02811-y.
103 S. Gandolfi, A. Sanouj, B. Chaput, A. Coste, B. Sallerin and A. Varin, *Biol. Direct*, 2024, **19**, 85, DOI: 10.1186/s13062-024-00534-6.
104 X. Song, Y. Chen, X. Chen, X. Zhao, Y. Zou, L. Li, X. Zhou, M. Li, D. Zhang, G. Ye, R. Jia and Z. Yin, *Int. J. Biol. Macromol.*, 2023, **244**, 125088, DOI: 10.1016/j.ijbiomac.2023.125088.
105 B. K. Utpal, B. Sutradhar, M. Zehravi, S. H. Sweilam, U. P. Panigrahy, D. Urs, A. F. Fatima, P. K. Nallasivan, G. S. Chhabra, M. Sayeed, M. A. Alshehri, S. O. Rab, S. L. Khan and T. B. Emran, *Naunyn-Schmiedeberg's Arch. Pharmacol.*, 2024, **398**, 2459–2485, DOI: 10.1007/s00210-024-03538-1.
106 X. T. Trinh, N. Van Long, L. T. Van Anh, P. T. Nga, N. N. Giang, P. N. Chien, S. Y. Nam and C. Y. Heo, *Int. J. Mol. Sci.*, 2022, **23**, 9573, DOI: 10.3390/ijms23179573.
107 L. Ou, X. Tan, S. Qiao, J. Wu, Y. Su, W. Xie, N. Jin, J. He, R. Luo, X. Lai, W. Liu, Y. Zhang, F. Zhao, J. Liu, Y. Kang and L. Shao, *ACS Nano*, 2023, **17**, 18669–18687, DOI: 10.1021/acsnano.3c03857.
108 V. Palmieri, M. Carmela Lauriola, G. Ciasca, C. Conti, M. De Spirito and M. Papi, *Nanotechnology*, 2017, **28**, 15, DOI: 10.1088/1361-6528/aa6150.

109 G. Qu, S. Liu, S. Zhang, L. Wang, X. Wang, B. Sun, N. Yin, X. Gao, T. Xia, J. J. Chen and G. B. Jiang, *ACS Nano*, 2013, **7**, 5732–5745, DOI: 10.1021/nn402330b.
110 M. Zhao, J. Shi, W. Cai, K. Liu, K. Shen, Z. Li, Y. Wang and D. Hu, *Int. J. Nanomed.*, 2021, **16**, 2647–2665, DOI: 10.2147/IJN.S300326.
111 M. Salama, Z. Alqarni, Y. S. Hamed, K. Yang, H. F. Nour and J. Lu, *J. Drug Delivery Sci. Technol.*, 2024, **95**, 105630, DOI: 10.1016/j.jddst.2024.105630.
112 X. Wang, L. Hao, C. Zhang, J. Chen and P. Zhang, *J. Biomater. Appl.*, 2017, **31**, 1108–1122, DOI: 10.1177/0885328216689364.
113 W. Sun, X. Zuo, Y. Zhang, C. Zhou, S. Guo, W. Li, M. Run and J. Qin, *Colloids Surf., B*, 2024, **244**, 114160, DOI: 10.1016/jcolsurfb.2024.114160.
114 N. Elhami, M. Pazhang, Y. Beygi-khosrowshahi and A. Dehghani, *Int. J. Biol. Macromol.*, 2024, **258**, 128832, DOI: 10.1016/j.ijbiomac.2023.128832.